

Cite this: *J. Mater. Chem. C*,
2024, 12, 8924

Prudently designed Se@fMWCNT as a peroxidase mimicking nanozyme for distinctive electrochemical detection of H₂O₂ and glutathione†

Vadakke Purakkal Sruthi  and Sellappan Senthilkumar *

Nanozymes are nanomaterials with enzymatic characteristics that are used to overcome the challenges associated with naturally occurring enzymes. A peroxidase mimicking nanozyme has been developed in this work, which has ability in the reduction of hydrogen peroxide (H₂O₂) to water, by oxidising the substrates in the presence of H₂O₂. We have designed and developed a neoteric Se@fMWCNT nanocomposite with peroxidase mimicking activity for electrochemical detection of H₂O₂ and glutathione (GSH). The choice of selenium (Se) was inspired by the natural enzymatic antioxidant glutathione peroxidase, which has Se as its active centre. Before preparation of the nanocomposite, MWCNT was functionalized with acid to obtain functionalized MWCNT, in order to improve biocompatibility and to increase conductivity by providing abundant active sites for the successful incorporation of Se. The as-synthesized nanocomposite was immobilized on a glassy carbon electrode, which could then be used for amperometric detection of the analytes H₂O₂ and GSH at neutral pH. The fabricated sensor exhibits a linear detection range of 50 nM–1.4 μM and a limit of detection (LOD) of 18.23 nM for H₂O₂, and a range of 50–450 μM and 500 μM–1.5 mM for GSH determination, with an LOD of 19.2 μM.

Received 27th March 2024,
Accepted 20th May 2024

DOI: 10.1039/d4tc01231c

rsc.li/materials-c

1. Introduction

Scrimin and Pasquato's team first coined the term 'nanozyme' in order to illustrate the ribonuclease-like activity of their gold nanoparticles functionalized with triazacyclononan.¹ Noticeably, following the discovery of intrinsic peroxidase mimetic characteristics of Fe₃O₄ by Yan and co-workers in 2007,² these nanozymes have been in the limelight in wide variety of areas of research, such as biomedicine, environmental monitoring and food safety.³ They have been exploited to replace the frailties of naturally occurring enzymes and existing artificially obtained/synthesized enzymes. Of several existing nanozymes, the four most explored nanozymes are for mimicking oxidase, peroxidase, catalase and superoxide dismutase (SOD), because of their vital role in biomedical science in protecting cells by altering the levels of reactive oxygen species (ROS) in the cells. Briefly, oxidases catalyse the oxidation of substrates by making use of oxygen (O₂) as the electron acceptor, eventually reducing O₂ to

water (H₂O) or hydrogen peroxide (H₂O₂). Similarly, SODs catalyse the conversion of superoxide into H₂O₂, which is further oxidised into H₂O and O₂. The decomposition of H₂O₂ into H₂O and O₂ is further aided by the enzyme catalase. Meanwhile, peroxidases oxidise substrates mostly in the presence of H₂O₂, where the substrates act as electron donors.^{4–6} Due to the outstanding catalytic properties of peroxidase enzymes, they are widely applied in diverse domains, including sensing, catalysis, bioimaging, and wound healing.^{3,7}

Peroxidase enzymes have acquired marked significance in bioscience due to their superior catalytic activity. They can oxidise a wide range of chromogenic substrates, such as *o*-phenylenediamine (OPD), 3,3',5,5'-tetramethylbenzidine (TMB), and 2,2'-azino-bis(3-ethylbenzthiazoline-6-sulphonic acid) (ABTS), in the presence of H₂O₂.^{2,8} They play a vital role in biological processes by efficiently detoxifying ROS and protecting cells from attack by pathogens. However, natural enzymes are prone to being denatured under harsh conditions, such as high temperature and variable pH. These limitations have given rise to peroxidase mimicking enzymes, or peroxidase nanozymes. Thus, natural peroxidases can be prudently substituted with peroxidase nanozymes for sustained bioanalytical applications in electrochemical, fluorescence and colorimetric sensing.^{9–11} Being a potent member of the ROS family, detection of H₂O₂ is crucial in order to monitor cell health. The optimum level of intracellular H₂O₂ should be less

Department of Chemistry, School of Advanced Sciences, Vellore Institute of Technology (VIT), Vellore-632014, India. E-mail: senthilkumar.s@vit.ac.in, senthilanalytical@gmail.com

† Electronic supplementary information (ESI) available: Effect of scan rate, electrocatalytic activity, amperometric curve (*i*-*t*) in different concentrations of H₂O₂, Lineweaver-Burk plot, stability studies. See DOI: <https://doi.org/10.1039/d4tc01231c>

than 10 nM. The presence of excessive H₂O₂ in cells is known to cause damage to the central nervous system, resulting in detrimental diseases, including cancer.¹² Hence, selective and sensitive detection of H₂O₂ is necessary to elevate quality of life.

Of late, several nanomaterials, especially carbon materials^{13–15} (graphene oxide (GO), multi-walled carbon nanotube (MWCNT), single-walled carbon nanotube (SWCNT), metal organic frameworks (MOFs),^{16–18} and nanomaterials,¹⁹ were identified for their ability to act as enzyme mimics. However, these materials have not yet been explored for electrochemical sensing in this context. Although there are numerous reports of peroxidase mimics for colorimetric sensing, only a handful of sensors have been reported as enzyme mimics in electrochemical sensing. However, these reported sensors have drawbacks, such as high sensing potential and failure to detect at neutral pH. Therefore, it is important to design and develop an enzyme mimicking material with superior analytical performance, in order to realize electrochemical detection in real-time, complex environments.

Glutathione (GSH) is a thiol-containing bioactive tripeptide, which consists of three amino acids, namely cysteine, glycine and glutamic acid.²⁰ GSH acts as an antioxidant that aids the enzyme glutathione peroxidase (GSHPx) in maintaining the intracellular and extracellular concentrations of H₂O₂.^{21,22} GSHPx protects the cells from oxidative damage by catalysing the reduction of H₂O₂. Selenium (Se) is the core moiety in GSHPx, which makes use of GSH as a cofactor in order to alter the oxidative damage caused by reactive oxygen species.^{23–26} The optimum level of GSH in blood should lie in the range 1–10 × 10^{−3} mol L^{−1} for a healthy individual.²⁷ Abnormal concentrations of GSH are known to cause several diseases, including cancers, diabetes, Parkinson's disease and Alzheimer's disease. Therefore, the detection of GSH is pivotal in order to ameliorate living standards.²⁸ Se present in GSHPx plays a pivotal role in its catalytic cycle and thus several Se-based nanozymes that act as GSHPx mimics have been reported, for diverse applications.²⁹ For example, Li and co-workers reported a selenium-doped g-C₃N₄ nanocomposite with peroxidase mimicking activity and used it for colorimetric detection of H₂O₂ and xanthine.³⁰ Later, in 2017, Huang *et al.* reported a GO-Se nanocomposite that acts as a GSHPx mimetic and used it for cytoprotection applications.³¹ Recently, Tian and co-workers synthesized a binuclear Fe-containing Se MOF nanozyme with tetraenzyme characteristics and successfully applied it as an antioxidant agent for the treatment of ischemic stroke.³² Although Se nanozymes and their efficacy have been investigated in detail, no attempts have been made, to the best of our knowledge, towards the electrochemical sensing of GSH, and this prompted us to develop a Se nanocomposite that could serve as a peroxidase mimic for the electrochemical determination of H₂O₂ and GSH subsequently.

MWCNTs are popular for their exceptional chemical stability, electronic conductivity, mechanical properties, moderate antibacterial nature and large surface to volume ratio, which have secured them a distinctive spot in sensing applications.^{33–39} Yet, they have downsides, such as poor solubilities and difficulties with regard to uniform dispersion, which could be overcome by functionalization of the MWCNTs. Introduction of functional

groups containing oxygen (–OH, –COOH and –C=O) by acid functionalization can lead to better dispersion and surface activation, thereby increasing the interfacial interactions between MWCNTs and other nanoparticles for the formation of nanocomposites.^{40–42}

Owing to the robust nature and ease of synthesis of nanozymes, they can act as substitutes for natural enzymes in disparate sensing applications. While natural enzymes are highly selective in nature, their activity depends on several parameters that include pH and temperature, making their application in sensors a tedious process. Taking into account the disadvantages of natural enzymes and significance of Se nanozymes, herein, we have fabricated a novel Se@fMWCNT peroxidase mimetic by a simple hydrothermal method. The functionalized MWCNT (fMWCNT) can serve as a host for Se as well as enhance the conducting properties of the nanocomposite. The synthesized material was employed for electrochemical sensing of H₂O₂ and GSH. Impressively, the developed sensor displayed wide linear ranges and low detection limits with high values of sensitivity towards both analytes.

2. Experimental section

2.1 Materials and methods

Selenium powder with approx. 100 mesh size and dopamine hydrochloride (DA) were purchased from Sigma Aldrich, India. Multi-walled carbon nanotubes, sodium phosphate monobasic anhydrous, sodium phosphate dibasic anhydrous, glutathione (GSH), uric acid (UA), tryptophan (L-Tryp), cholesterol (Chol), cystine (Cys), glucose (Glu) and potassium chloride (KCl) were acquired from SRL Chemicals, India. Leucine (Leu) was acquired from Sd Fine Chemicals, India. Hydrogen peroxide (H₂O₂) and ascorbic acid (AA) were purchased from Merck, India. Potassium perchlorate (KClO₃) was obtained from Alfa Aesar, India, and potassium nitrite (KNO₃) was bought from Avra Chemicals, India. Valine (Val) was purchased from Spectrochem, India. Glutone-Hydra tablets containing L-GSH were obtained from CRIUS life sciences and milk samples were obtained from a local vendor. All the chemicals obtained were of analytical grade and used without further purification. Milli-Q water was used to prepare all the sample solutions.

2.2 Instrumentation

Powder X-ray diffraction (PXRD) spectra were obtained using a Bruker D8 advance instrument with iron-filtered Cu K α radiation ($\lambda = 1.5406 \text{ \AA}$). Field emission scanning electron microscopy (FESEM) analysis was carried out on a Thermo-Fisher FEI QUANTA 250 FEG under high vacuum conditions, at an operating voltage range of 5–30 kV. High-resolution transmission electron microscopy (HR-TEM) studies were performed on a JEOL JEM 2100 with LaB₆ as the electron source. X-ray photoelectron spectroscopic (XPS) studies were carried out using a PHI5000 Version Probe III. All electrochemical studies were performed using a CHI-760E electrochemical workstation. A conventional three-electrode system, with glassy carbon

electrode (GCE) as the working electrode, Ag/AgCl as the reference electrode and platinum coil as the counter electrode, was used to perform the electrochemical studies.

2.3 Functionalization of MWCNT

MWCNT was acid-functionalized using a previously reported literature method with minor modifications.⁴³ Typically, 1 g of MWCNT was added into a round-bottomed flask consisting of a mixture of 20 mL HNO₃ and 60 mL H₂SO₄, and the mixture was refluxed for 6 hours at 80 °C (Scheme 1). Later, the resultant mixture was washed continuously with distilled water until the filtrate attained a neutral pH value. Thereafter, the obtained sample was centrifuged and later dried overnight at 60 °C to obtain fMWCNT.

2.4 Synthesis of Se@fMWCNT nanocomposite

After a few attempts, the procedure for the synthesis of Se@fMWCNT nanocomposite as a peroxidase mimic was optimized (Scheme 1) and is as follows. Initially, 200 mg of Se powder and 100 mg of fMWCNT were sonicated separately in 35 mL of H₂O for 30 minutes, and then, the solutions were mixed and sonicated for 30 minutes. The concomitant mixture was taken in a 100 mL autoclave and heated for 12 hours at 120 °C. Then, the obtained precipitate was centrifuged multiple times with water and ethanol and was allowed to dry in a hot air oven at 60 °C overnight to attain Se@fMWCNT.

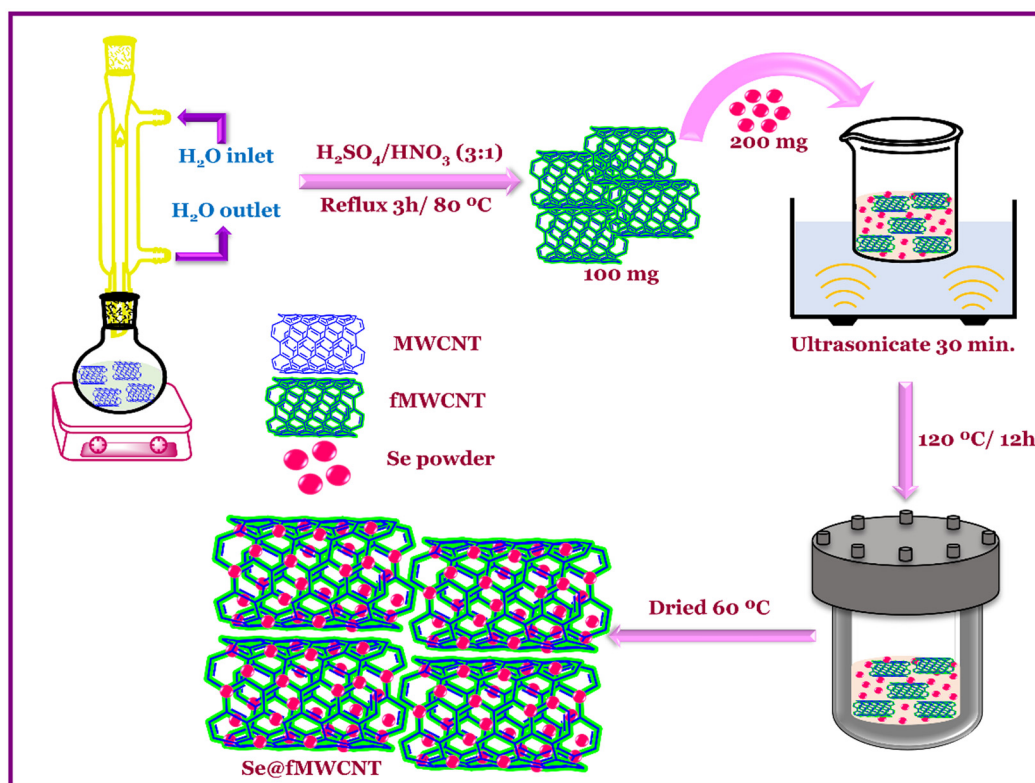
2.5 Modification of working electrode

To begin with the GCE was polished with slurries of alumina of size 1 μm, 0.3 μm and 0.05 μm. Then, 10 μL of Se@fMWCNT (1 mg in 50 μL EtOH, 49 μL H₂O and 1 μL Nafion) was drop-coated onto the pre-cleaned GCE and allowed to dry at room temperature to obtain Se@fMWCNT/GCE. Prior to performing the electrochemical studies, Se@fMWCNT/GCE was stabilized by conducting cyclic voltammetry (CV) in the potential range +0.2 to −0.8 V (vs. Ag/AgCl electrode).

3. Results and discussion

3.1 Characterization of Se@fMWCNT

The formation of Se@fMWCNT nanocomposite has been investigated by recording the PXRD patterns of Se powder, fMWCNT and Se@fMWCNT, and the patterns are shown in Fig. 1a. The peaks at 23.4°, 29.6°, 41.1°, 43.6°, 45.2°, 51.4° and 55.8° are attributed to the (100), (101), (110), (102), (100), (201) and (112) planes of Se (blue curve) (JCPDS 06-0362). The XRD pattern of fMWCNT (green curve) shows two peaks at 25.8° and 42.6°, which can be correlated to the (002) and (100) planes, respectively, corresponding to graphitic carbon. The formation of Se@fMWCNT nanocomposite (orange curve) was confirmed with the appearance of an additional peak at 26.2° representing the (002) plane of fMWCNT along with the characteristic peaks of Se. Due to the higher intensity of the (102) plane of Se, the peak at 42.6° corresponding to the (100) plane of fMWCNT has



Scheme 1 Schematic diagram of synthesis of Se@fMWCNT.

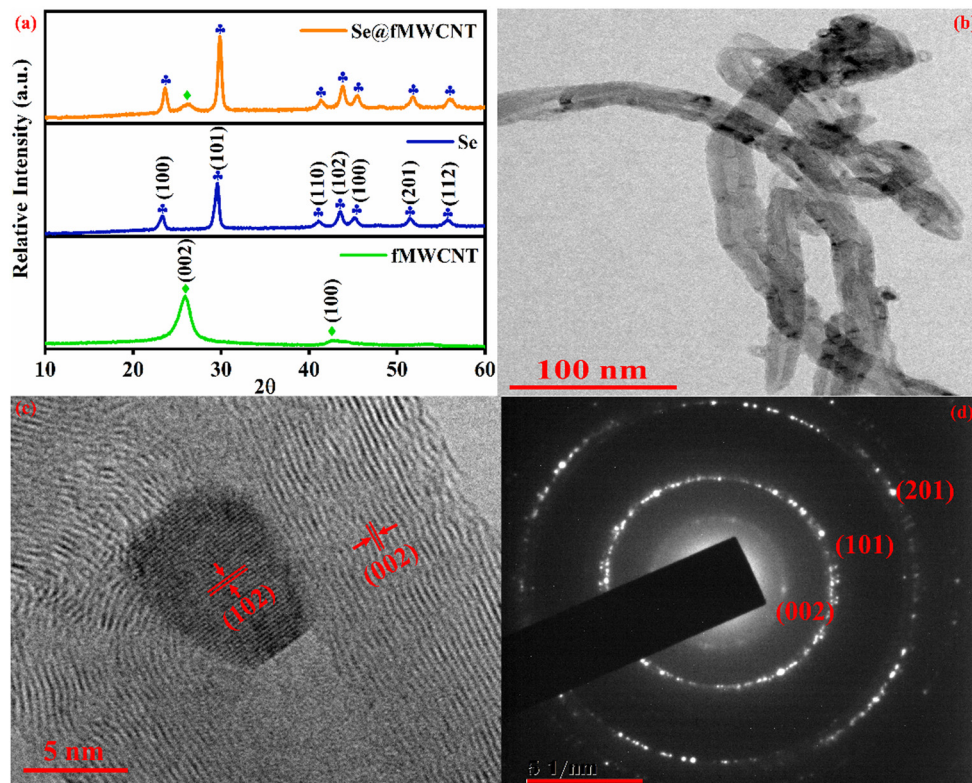


Fig. 1 (a) XRD patterns of fMWCNT (green), Se (blue) and Se@fMWCNT (orange). (b) and (c) HR-TEM images and (d) SAED pattern of Se@fMWCNT.

diminished in the nanocomposite. Additionally, the HR-TEM images (Fig. 1b and c) and selected area electron diffraction (SAED) pattern (Fig. 1d) support that Se has been successfully

anchored onto the fMWCNT. Fig. 1c shows the HR-TEM image of Se@fMWCNT and exhibits d -spacings of 0.26 nm and 0.33 nm, which can be attributed to the (102) and (002) planes.

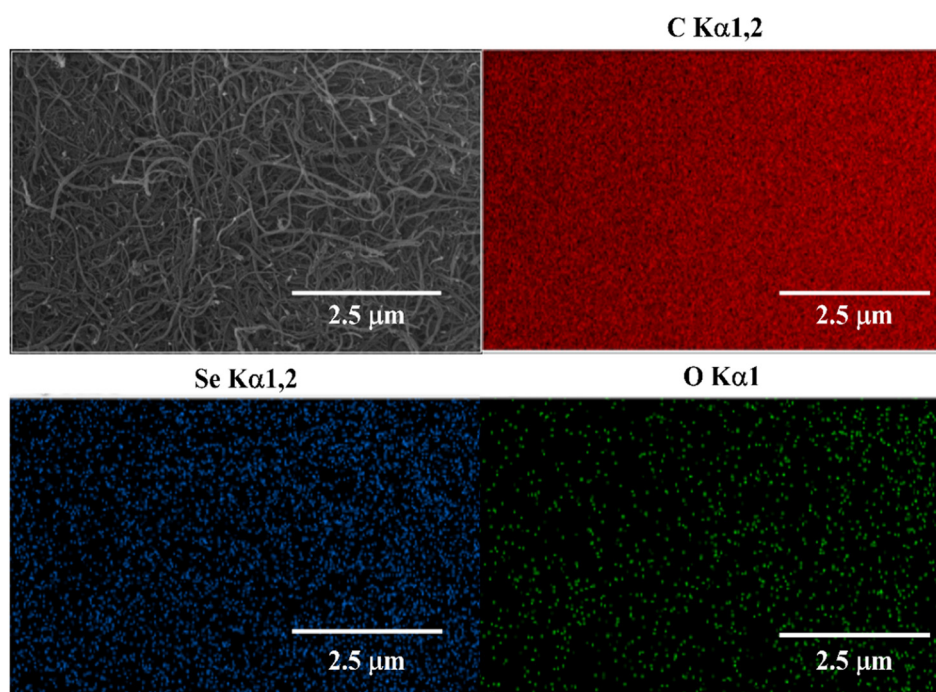


Fig. 2 FESEM and elemental analysis of Se@fMWCNT nanocomposite.

In addition, Fig. 1d discloses the SAED pattern, consisting of rings that can be assigned to the amorphous nature of fMWCNT (002) and crystalline nature of Se atoms, which can be indexed to the (101) and (201) planes. Moreover, the size of the Se nanoparticles on fMWCNT was obtained from the HR-TEM images, with the average size of Se found to be 7.9 nm. Furthermore, the morphology of the prepared Se@fMWCNT was probed using FESEM and elemental mapping, and the results are displayed in Fig. 2. The FESEM images show the uniform size of the Se nanoparticles, and the elemental mapping proved that the elements are uniformly distributed.

The surface composition of Se@fMWCNT (Fig. 3a) was identified using XPS, which reveals the presence of Se, carbon (C) and oxygen (O). In the Se 3d spectrum (Fig. 3b), the two major peaks at binding energy (B.E.) values of 55.7 eV and 54.8 eV represent the 3d_{3/2} and 3d_{5/2} states of Se, affirming the -2 oxidation state.^{44–46} The small peaks at 56.5 eV and 58.4 eV are due to the formation of C–Se bonds.^{45,47} The O 1s spectrum (Fig. 3c) shows the presence of C–OH at a B.E. value of 533.48 eV, HO–C=O at a B.E. value of 532.58 eV and C=O at a B.E. value of 531.38 eV.^{48,49} The deconvoluted spectrum of C 1s (Fig. 3d) unravels the presence of functional groups, such as C–O, C=O and COOH. The peaks at B.E. values of 284.48 eV and 284.98 eV could be assigned to C=C (sp²) and C–C/C–Se (sp³), respectively.^{50,51} The peaks correlating to C–O species are found to occur between 286 and 289 eV, and the satellite peak around 291 eV could be assigned to the π–π* transition.⁵⁰ Thus, the XPS results clearly infer the formation of Se@fMWCNT, which could subsequently be used for electrochemical detection.

3.2 Electrochemical and electrocatalytic behaviour of Se@fMWCNT/GCE

The electrochemical behaviour of the newly synthesized nanocomposite has been probed using CV. As anticipated, the Se@fMWCNT/GCE did not exhibit any redox activity in 0.1 M PBS (pH = 7; N₂ saturated) in the potential window from -0.2 V to +0.8 V. Since redox behaviour was not observed for Se@fMWCNT/GCE, the scan rate effect was studied in the presence of a 2.5 mM ferricyanide/ferricyanide redox couple. Both oxidation and reduction peak currents showed a gradual increment with increase in the scan rate. As shown in Fig. S1 (ESI[†]), the square root of scan rate *vs.* peak current had a linear relationship, indicating that the redox process occurring at the modified electrode surface is diffusion controlled. The electrochemical active surface area (ECSA) of the Se@fMWCNT/GCE and fMWCNT/GCE were also calculated using the Randles–Sevcik equation,^{52–54} as displayed below:

$$i_p = 2.69 \times 10^5 \times A \times C \times n^{3/2} \times D^{3/2} \times \nu^{3/2},$$

where i_p (A) is the anodic peak current, A (cm²) is the ECSA, C (mol cm⁻³) is the concentration of Fe³⁺ ions, n is the number of electrons involved in the redox process, D (cm² s⁻¹) is the diffusion coefficient of Fe³⁺ and ν (V s⁻¹) is the scan rate. The ECSA was obtained from the slope of the square root of scan rate *vs.* current and was calculated to be 0.251 cm² for Se@fMWCNT/GCE and 0.031 cm² for fMWCNT/GCE. Furthermore, the electrocatalytic activity of the Se nanozyme sensor was explored for H₂O₂ sensing, and the voltammetric response of bare GCE and Se@fMWCNT/GCE in the absence and presence

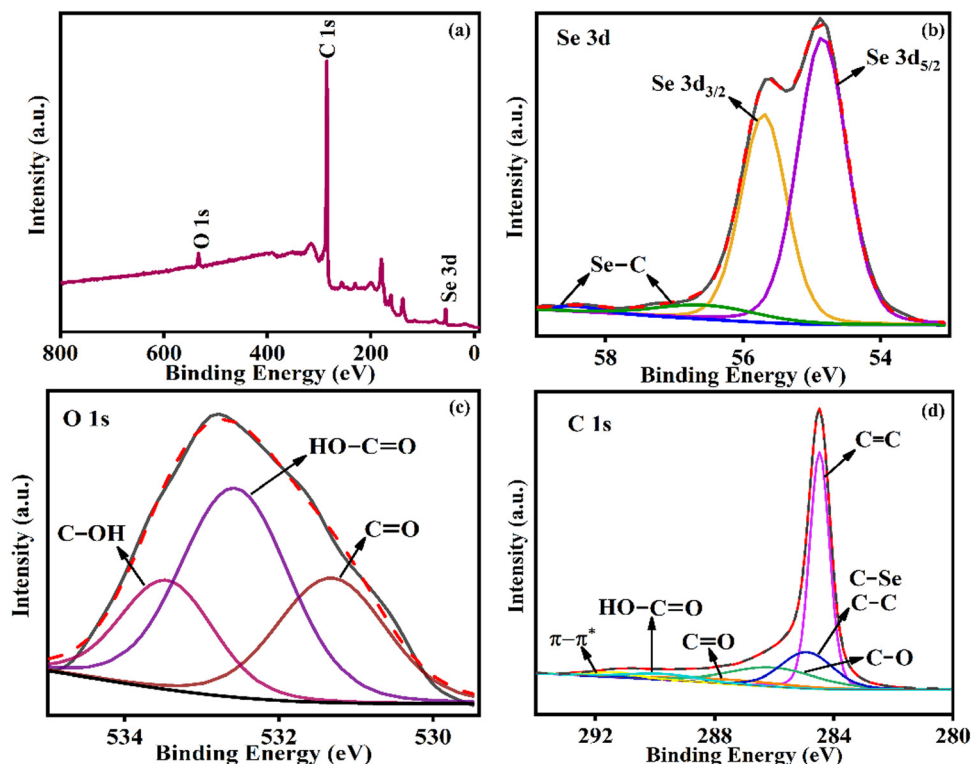


Fig. 3 (a) XPS survey spectrum of Se@fMWCNT and core-level spectra of (b) Se 3d, (c) O 1s and (d) C 1s.

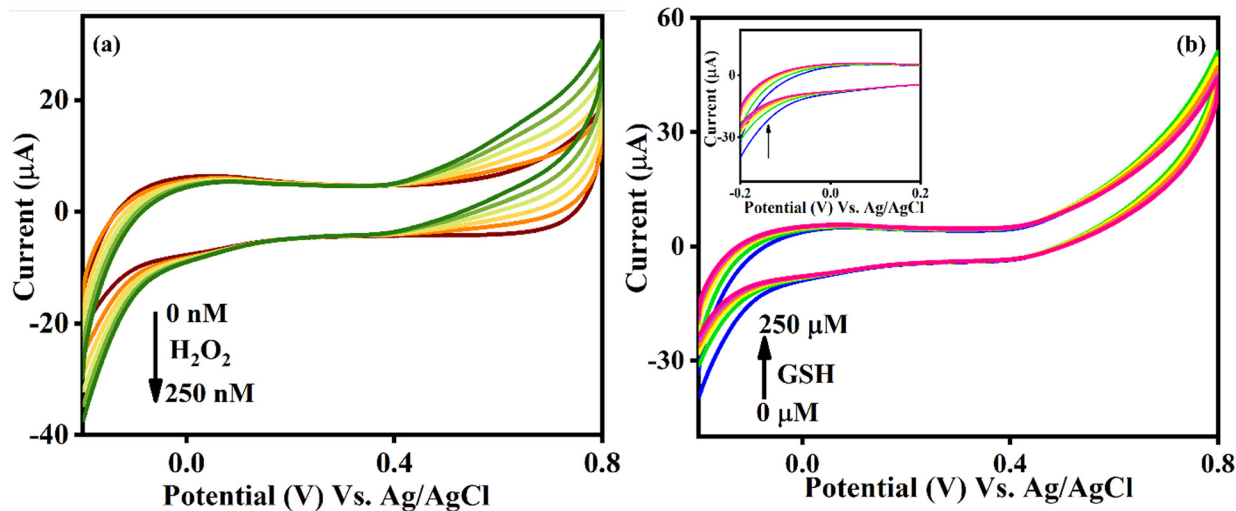


Fig. 4 CV response of Se@fMWCNT/GCE in 0.1 M PBS (pH = 7; N₂ saturated) at a scan rate of 50 mV s⁻¹ for (a) increasing concentration of H₂O₂ (0–250 nM) and (b) increasing concentration of GSH in the presence of 1 mM H₂O₂ (0–250 μM).

of H₂O₂ are depicted in Fig. S2 (ESI[†]). The bare GCE did not show any response towards H₂O₂. However, as shown in Fig. 4a the Se@fMWCNT/GCE showed a prominent linear increment in cathodic current around -0.2 V on successive additions of 50 nM H₂O₂. Subsequently, in order to study the electrocatalytic activity of Se@fMWCNT towards GSH, 50 μM of GSH solution was added to 0.1 M PBS (pH = 7; N₂ saturated) consisting of 1 mM H₂O₂ (Fig. 4b). Although there was no formation of a redox peak, interestingly the cathodic tail currents at -0.2 V decreased linearly, indicating the oxidation of GSH to its oxidised form of GSSH. The exciting electrocatalytic behaviour of the Se@fMWCNT modified electrode can be attributed to the deliberate choice of Se metal and fMWCNT and to optimization of the electrochemical parameters.

3.3 Amperometric detection of H₂O₂ and GSH

The impressive electrocatalytic activity of Se@fMWCNT/GCE towards H₂O₂ and GSH prompted us to investigate its performance

under dynamic conditions using the amperometric technique. Hence, amperometric measurements were carried out in N₂-saturated 0.1 M PBS (pH = 7) with an operating potential of -0.2 V and solution rotation speed of 350 rpm. Fig. 5a shows the amperometric (*i*-*t*) curve of Se@fMWCNT/GCE for different concentrations of H₂O₂ spiked at an addition time interval of 50 s. The Se@fMWCNT/GCE shows a uniform catalytic current response for successive addition of 50 nM H₂O₂, which clearly depicts the tremendous peroxidase enzyme mimicking property of the fabricated sensor obtained, resulting from the selection of Se metal and fMWCNT. The corresponding calibration plot (Fig. 5b) displays exceptional linearity in the concentration range from 50 nM to 1.4 μM with a regression coefficient (*R*²) value of 0.9992. The detection limit and sensitivity of Se@fMWCNT/GCE towards H₂O₂ sensing were found to be impressively, as 18.23 nM and 0.1585 μA μM⁻², respectively. The linear range, detection limit and sensitivity thus obtained using Se@fMWCNT/GCE for the

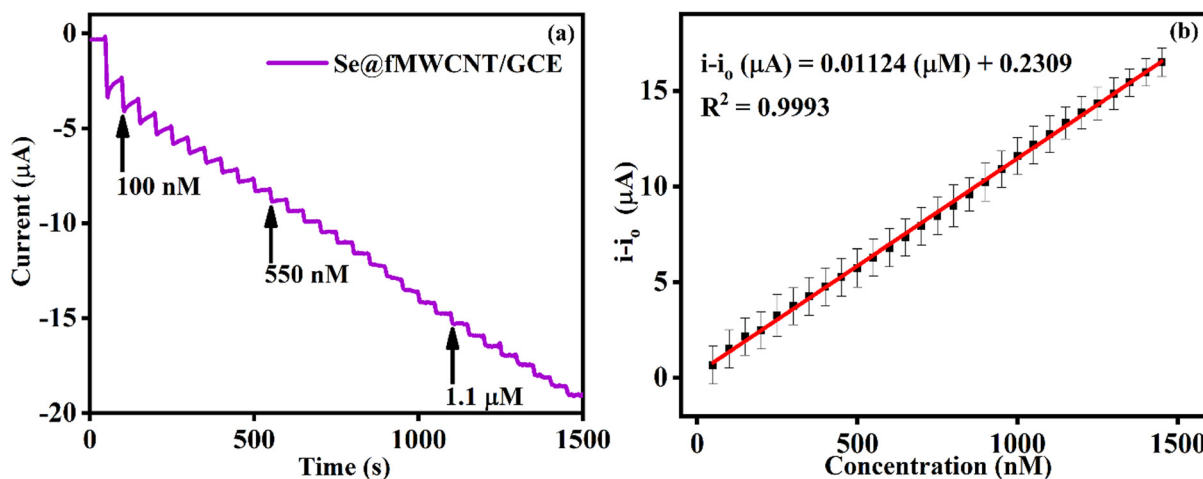
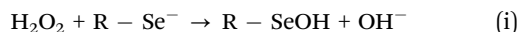


Fig. 5 (a) Amperometric response of Se@fMWCNT/GCE for sequential addition of H₂O₂ in 0.1 M PBS (pH = 7; N₂ saturated) at -0.2 V. (b) Calibration plot obtained from amperometric response.

detection of H_2O_2 are comparable or better than for other recently reported nanozyme-based H_2O_2 sensors.^{55–58}

Similarly, GSH was detected amperometrically in 0.1 M PBS (pH = 7; N_2 saturated) consisting of 1 mM H_2O_2 . The operating potential was fixed at -0.2 V, and the solution was stirred at 350 rpm, and, as expected, a linear decrease in current was observed for every addition of GSH. This decrease in catalytic current is due to the oxidation of GSH to GSSH, and the sudden increase in current response is because of the availability of large numbers of active sites at Se@fMWCNT/GCE. The experiment was also carried out in the absence and presence of varying concentrations of H_2O_2 (0.1 mM, 1 mM and 10 mM), and the results are presented in Fig. S3 (ESI[†]). As anticipated, no reasonable difference in current was seen in the absence of H_2O_2 (Fig. S3a, ESI[†]) and a significant decrease in current response was noted in the presence of H_2O_2 (Fig. S3(b–d), ESI[†]). These results clearly infer that the Se@fMWCNT sensor detected GSH only when H_2O_2 is present, revealing that the sensor demonstrates GSHPx-like characteristics. Although obvious decrease in the current response was noticed at different concentrations of H_2O_2 , a distinct and linear response was obtained only in the presence of 1 mM H_2O_2 (Fig. S3c, ESI[†]) and hence this concentration was chosen as the optimum concentration for amperometric determination of GSH (Fig. 6a). The mechanism of sensing of GSH is similar to that observed in the enzyme GSHPx and can be expressed as follows:



The first step involves the formation of a selenic acid derivative (R–SeOH) by oxidation of R–Se[−] and generation of OH[−] anion by the reduction of H_2O_2 . In the second step, R–SeOH reacts with the added analyte GSH and forms the selenyl-sulfide intermediate (R–Se–SG) and H_2O . Then, in the

third step, the R–Se–SG intermediate immediately reacts with another molecule of GSH to form GSSH, during which R–Se[−] is regenerated. These reactions occur in a cycle as long as the analyte GSH is available at the electrode surface, which results in a linear current response. The calibration plot corresponding to the amperometric response obtained is shown in Fig. 6b. The developed sensor had two linear ranges, from 50 to 450 μM and from 500 μM to 1.5 mM, and the LOD was calculated to be 19.2 μM . The sensitivities of the Se@fMWCNT/GCE sensor towards GSH detection were calculated to be 0.1465 and 0.2873 $\mu\text{A} \mu\text{M}^{-1} \text{cm}^{-2}$. The obtained analytical parameters are comparable or better than for the recently reported sensors for GSH detection.^{27,28,57,59–61} Furthermore, fMWCNT/GCE was employed for its ability to detect H_2O_2 and GSH as shown in Fig. S4(a and b) (ESI[†]). In detail, 50 nM of H_2O_2 was added to a solution of N_2 -saturated 0.1 M PBS (pH = 7) at a time interval of 50 s. Similarly, 50 μM of GSH was added to a solution of N_2 -saturated 0.1 M PBS (pH = 7) containing 1 mM H_2O_2 at a time interval of 50 s. From the figures it can be seen that fMWCNT/GCE (without Se) does not show any linear or reproducible response, and hence it cannot be employed for detection of H_2O_2 and GSH. This investigation also evidences that the enzyme mimicking activity could not be observed in the absence of Se and is attained only with Se@fMWCNT/GCE.

3.4 Peroxidase mimetic activity of Se@fMWCNT

The Michaelis–Menten constants (K_m and I_{max}) are important in the case of biological enzymatic systems, as they provide vital information about the magnitude of the affinity between the enzyme and substrate. Lower values of K_m indicate effective binding of the enzyme to the substrate and a higher value of I_{max} implies the better catalytic activity of the enzyme. Hence, the enzyme mimicking efficacy of the newly designed nanozymes could be understood by comparing these parameters with those of natural enzymes. The peroxidase-like activity of nanozymes can be evaluated by their ability to oxidise substrates such as TMB, ABTS, and OPD, in the presence of

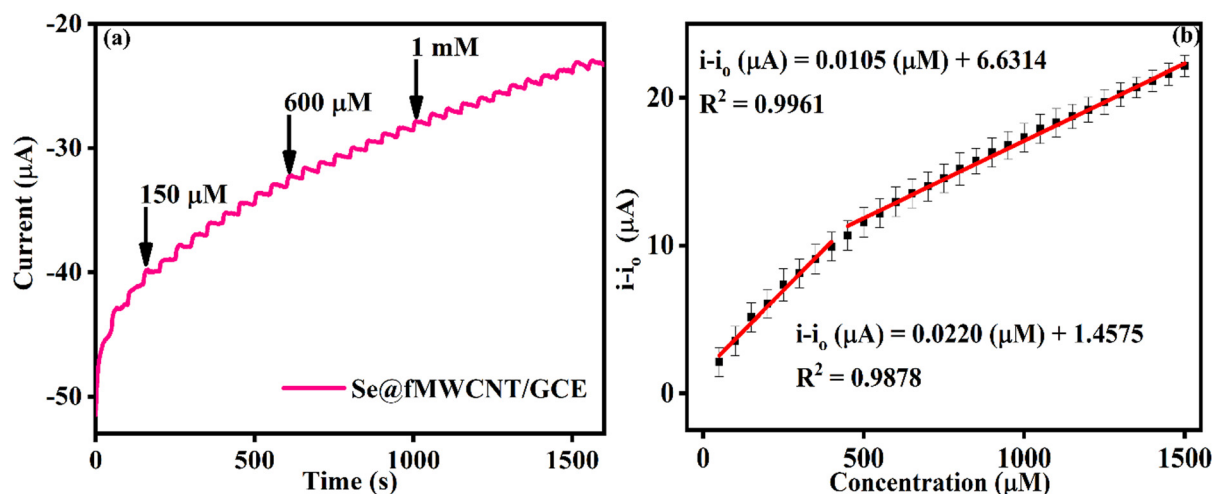


Fig. 6 (a) Amperometric response of Se@fMWCNT/GCE for successive addition of GSH in 0.1 M PBS (pH = 7; N_2 saturated) containing 1 mM of H_2O_2 at -0.2 V. (b) Calibration plot obtained from amperometric response.

H_2O_2 .^{62–64} Herein, the peroxidase mimicking characteristics of Se@fMWCNT were assessed primarily using UV-vis spectroscopy.⁶³ Precisely, to a solution containing 1 mM H_2O_2 in 0.1 M PBS (pH = 7), 1 mg TMB and 1 mg mL^{-1} of the synthesized Se@fMWCNT were added (Fig. S5a inset, ESI[†]). As expected, the colour of the solution changed to blue, indicating the peroxidase mimicking activity of the synthesized Se@fMWCNT nanocomposite. Furthermore, on addition of 1 mM GSH, the solution turned colourless, restricting the further oxidation of TMB by Se@fMWCNT. The UV-vis spectrum (Fig. S5a, ESI[†]) of TMB in 1 mM H_2O_2 showed a weak absorbance, which was enhanced upon addition of 1 mg of Se@fMWCNT, proving the ability of Se@fMWCNT to oxidise TMB. Moreover, on introduction of 1 mM GSH to the aforementioned solution, the absorbance diminished, since GSH acts as a reductant, prohibiting further oxidation of TMB by the Se@fMWCNT nanocomposite.⁶⁵ Furthermore, the peroxidase mimicking efficacy of the Se@fMWCNT nanozyme has been examined using amperometric measurements, and the Michaelis–Menten parameters were

quantified using the Lineweaver–Burk equation, as follows:⁶⁶

$$\frac{1}{I} = \frac{K_m}{I_{\max}} \frac{1}{C} + \frac{1}{I_{\max}}$$

where I represents anodic or cathodic current, C represents the concentration of analyte and I_{\max} is the maximum electrocatalytic current. K_m and I_{\max} were calculated from the $1/I$ versus $1/C$ plots of H_2O_2 (Fig. S5b, ESI[†]) and were found to be 4.42 μM and 60.98 μA , respectively. The K_m value of Se@fMWCNT nanocomposite with H_2O_2 as substrate was found to be remarkably less than that of the natural horseradish peroxidase (HRP) enzyme, which is indicative of a larger affinity of the synthesized nanocomposite towards H_2O_2 .²

3.5 Interference and stability studies

With the aim of investigating the selectivity for the real-time applicability of the constructed sensor towards electrochemical determination of H_2O_2 and GSH, the effect of interferents was also studied by performing amperometry in 0.1 M PBS (pH = 7),

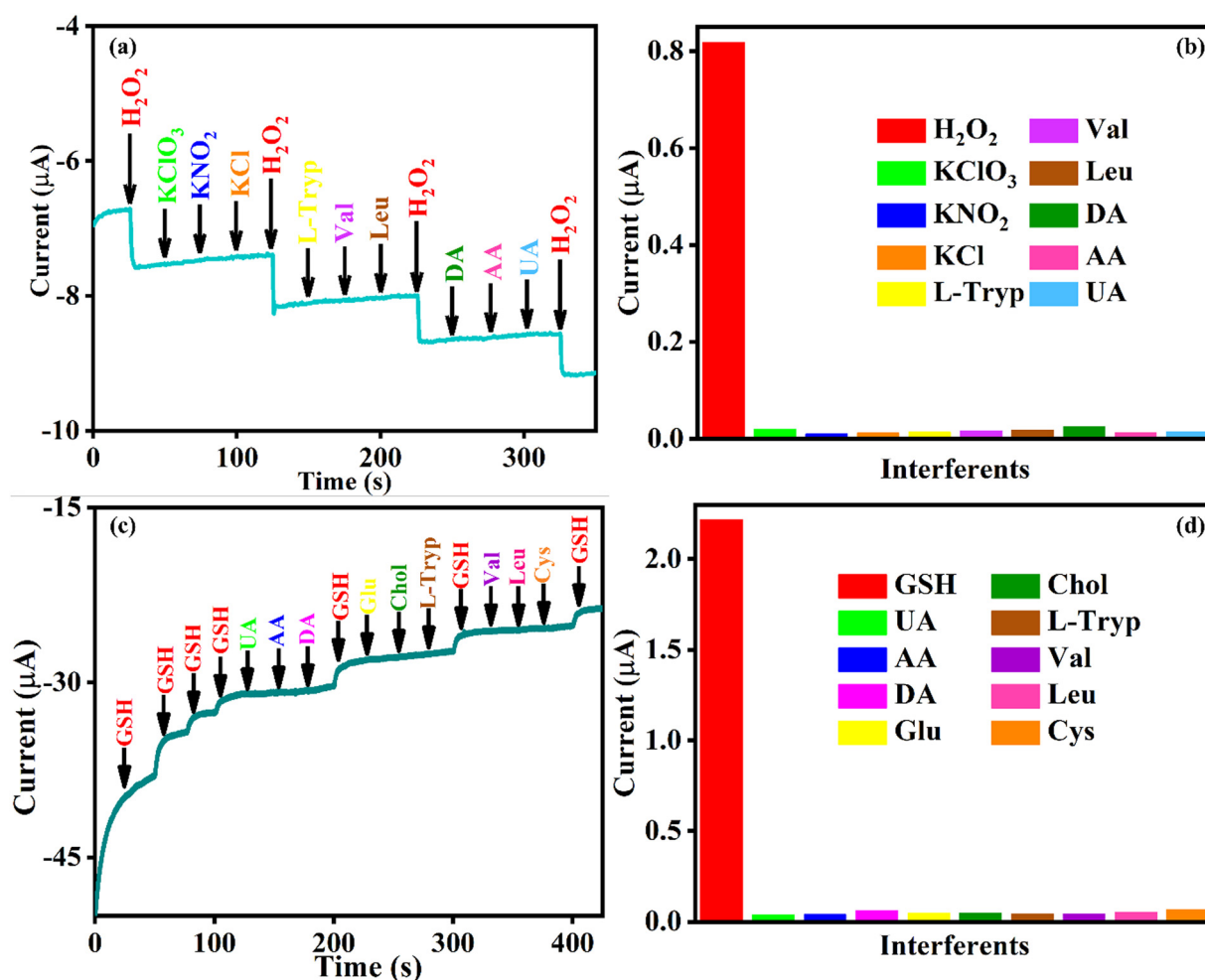


Fig. 7 (a) Effect of interferents on the amperometric response of Se@fMWCNT/GCE towards 50 nM H_2O_2 in 0.1 M PBS (pH = 7; N_2 saturated). (b) Columnar diagram of corresponding current response. (c) Effect of interferents on the amperometric response of Se@fMWCNT/GCE towards 50 μM GSH in 0.1 M PBS (pH = 7; N_2 saturated) containing 1 mM H_2O_2 . (d) Columnar diagram of corresponding current response.

Table 1 Real-time analysis of H₂O₂ in milk and GSH in tablet samples

Sample	Spiked	Found ^a	Recovery (%)
Milk	100 nM	97.8 ± 1 nM	97.8
	200 nM	206.2 ± 2 nM	103.1
Glutone-Hydra tablet	100 μM	98.1 ± 2 μM	98.1
	200 μM	203.9 ± 1 μM	101.9

^a Triplicates were performed.

at an applied potential of -0.2 V. The interfering species, namely, KClO₃, KNO₂, L-Tryp, Val, Leu and Cys, were chosen since they have high tendency to interfere with H₂O₂ and GSH at an applied potential of -0.2 V. Further, DA, UA, AA, Chol and Glu are some well-known interfering species in biological systems, and hence were used as interferents in order to study the selectivity of the sensor. Fig. 7a shows the amperometric current response of Se@fMWCNT/GCE towards H₂O₂ along with a tenfold excess of other, concomitant interfering species. The corresponding columnar diagram of the current response (Fig. 7b) depicts that the developed sensor is highly selective towards H₂O₂. Similarly, the selectivity of Se@fMWCNT/GCE towards GSH was determined by carrying out amperometry at -0.2 V in 0.1 M PBS comprising of 1 mM H₂O₂. Fig. 7c shows the amperometric current response of Se@fMWCNT/GCE towards GSH along with a tenfold excess of other interferents. The respective columnar diagram of the current response (Fig. 7d) illustrates the high selectivity of Se@fMWCNT/GCE towards GSH, since no, or negligible, signal was obtained for any other interferents. The results clearly validate that the Se@fMWCNT/GCE sensor has exceptional selectivity towards biomimetic electrochemical detection of H₂O₂ and GSH.

The stability of this newly proposed nanozyme-based sensor was also probed by recording cyclic voltammetry at a scan rate of 50 mV s⁻¹ for 100 continuous cycles in 0.1 M PBS (pH = 7; N₂ saturated), and the results are shown in Fig. S6 (ESI[†]). Fig. S6 (ESI[†]) clearly demonstrates that the constructed sensor was stable up to 100 cycles without any decline in current response, both in the absence and presence of 1 mM H₂O₂. The stability studies confirm the robust, lasting nature of the sensing probe Se@fMWCNT, which is an essential quality for real-time applications.

3.6 Real-time analysis

The sensor was tested for its ability to detect H₂O₂ and GSH in real-time samples. For this purpose, the fabricated sensor was employed towards sensing of H₂O₂ and GSH in milk samples and glutathione tablets, respectively, and this is shown in Fig. S7(a and b) (ESI[†]). Briefly, milk samples were diluted using 0.1 M PBS (pH = 7) and a known concentration of H₂O₂ was spiked by a standard addition method. Similarly, GSH tablets were diluted to 10 mM using 0.1 M PBS (pH = 7) and a known concentration was spiked to a solution of 0.1 M PBS (pH = 7), consisting of 1 mM H₂O₂. All the measurements were carried out in triplicate, and the fabricated sensor showed a good

recovery percentage and low RSD values, as presented in Table 1.

4. Conclusion

In summary, a simple viable Se@fMWCNT nanocomposite with intrinsic peroxidase mimicking activity has been synthesized via a hydrothermal method. The as-prepared nanocomposite showed excellent nanozyme activity and was utilized to construct an electrochemical biosensor for the determination of H₂O₂ and GSH. The system shows extraordinary Michaelis–Menten values, which reveals the unprecedented peroxidase-like activity. The Se@fMWCNT/GCE sensor functions by electrochemical reduction of H₂O₂ and subsequently facilitates the electrochemical oxidation of GSH. Selectivity of the sensor towards H₂O₂ and GSH was achieved by appropriate selection of Se and the presence of fMWCNT. In addition, fMWCNT served as a good host for Se and enhanced the conductivity, thereby contributing significantly towards the peroxidase activity of the sensor. Furthermore, the Se@fMWCNT/GCE sensor is expected to show a sensing mechanism with close resemblance to the naturally occurring GSHPx enzyme. This work exemplifies a new, simple and judiciously designed nanocomposite as an enzyme mimic, with outstanding peroxidase mimicking activity for the selective detection of H₂O₂ and GSH. The present investigation also opens up an avenue towards the design and engineering of novel nanomaterials with biomimetic activity for application in bioelectrocatalysis, clinical diagnosis and environmental screening.

Author contributions

Vadakke Purakkal Sruthi: conceptualization, methodology, investigation, validation, writing – original draft. Sellappan Senthilkumar: conceptualization, resources, supervision, project administration, writing – review & editing.

Conflicts of interest

There are no conflicts to declare.

References

- 1 D. Jiang, D. Ni, Z. T. Rosenkrans, P. Huang, X. Yan and W. Cai, *Chem. Soc. Rev.*, 2019, **48**, 3683–3704.
- 2 L. Gao, J. Zhuang, L. Nie, J. Zhang, Y. Zhang, N. Gu, T. Wang, J. Feng, D. Yang, S. Perrett and X. Yan, *Nat. Nanotechnol.*, 2007, **2**, 577–583.
- 3 B. Das, J. Lou Franco, N. Logan, P. Balasubramanian, M. Il Kim and C. Cao, *Nanozymes in Point-of-Care Diagnosis: An Emerging Futuristic Approach for Biosensing*, *Nano-Micro Lett.*, 2021, **13**, 193.
- 4 Y. Huang, J. Ren and X. Qu, *Chem. Rev.*, 2019, **119**, 4357–4412.
- 5 H. Wei and E. Wang, *Chem. Soc. Rev.*, 2013, **42**, 6060–6093.
- 6 J. Wu, X. Wang, Q. Wang, Z. Lou, S. Li, Y. Zhu, L. Qin and H. Wei, *Chem. Soc. Rev.*, 2019, **48**, 1004–1076.

- 7 N. Waris, A. Hasnat, S. Hasan, S. Bano, S. Sultana, A. O. Ibhaddon and M. Z. Khan, *J. Mater. Chem. B*, 2023, **11**, 6762–6781.
- 8 L. X. Yn, B. B. Wang, X. Zhao, L. J. Chen and X. P. Yan, *ACS Appl. Mater. Interfaces*, 2021, **13**, 60955–60965.
- 9 M. Bilal, N. Khaliq, M. Ashraf, N. Hussain, Z. Baqar, J. Zdarta, T. Jesionowski and H. M. N. Iqbal, *Colloids Surf., B*, 2023, **221**, 112950.
- 10 Q. Wang, H. Wei, Z. Zhang, E. Wang and S. Dong, *TrAC, Trends Anal. Chem.*, 2018, **105**, 218–224.
- 11 Z. Chen, Y. Yu, Y. Gao and Z. Zhu, *ACS Nano*, 2023, **17**, 13062–13080.
- 12 D. Mohanapriya, J. Satija, S. Senthilkumar, V. Kumar Ponnusamy and K. Thenmozhi, *Coord. Chem. Rev.*, 2024, **507**, 215746.
- 13 Y. Song, X. Wang, C. Zhao, K. Qu, J. Ren and X. Qu, *Chem. – Eur. J.*, 2010, **16**, 3617–3621.
- 14 H. Sun, Y. Zhou, J. Ren and X. Qu, *Angew. Chem.*, 2018, **130**, 9366–9379.
- 15 X. Wang, H. Wang and S. Zhou, *J. Phys. Chem. Lett.*, 2021, **12**, 11751–11760.
- 16 D. Wang, D. Jana and Y. Zhao, *Acc. Chem. Res.*, 2020, **53**, 1389–1400.
- 17 X. Niu, X. Li, Z. Lyu, J. Pan, S. Ding, X. Ruan, W. Zhu, D. Du and Y. Lin, *Chem. Commun.*, 2020, **56**, 11338–11353.
- 18 X. Huang, S. Zhang, Y. Tang, X. Zhang, Y. Bai and H. Pang, *Coord. Chem. Rev.*, 2021, **449**, 214216.
- 19 Y. Lin, J. Ren and X. Qu, *Acc. Chem. Res.*, 2014, **47**, 1097–1105.
- 20 J. Nemhauser and J. Chory, *Arab. B.*, 2002, **2011**, 1–32.
- 21 H. Ungati, V. Govindaraj, M. Narayanan and G. Mugesh, *Angew. Chem., Int. Ed.*, 2019, **58**, 8156–8160.
- 22 A. Iqbal, A. Khan, A. laeeq, K. Malhotra, M. A. Ansari and S. E. Haque, *Curr. Pharm. Des.*, 2021, **27**, 3881–3900.
- 23 J. Chaudiere, O. Courtin and J. Leclaire, *Arch. Biochem. Biophys.*, 1992, **296**, 328–336.
- 24 G. S. Heverly-Coulson and R. J. Boyd, *J. Phys. Chem. A*, 2010, **114**, 1996–2000.
- 25 R. Brigelius-Flohé and M. Maiorino, *Biochim. Biophys. Acta, Gen. Subj.*, 2013, **1830**, 3289–3303.
- 26 S. Ghosh, P. Roy, N. Karmodak, E. D. Jemmis and G. Mugesh, *Angew. Chem., Int. Ed.*, 2018, **57**, 4510–4515.
- 27 G. Liu, T. Xia, J. Wei, S. Hou and S. Hou, *ChemElectroChem*, 2022, **9**, 1–8.
- 28 T. Zhang, N. Lu, C. Wang, H. Jiang, M. Zhang, R. Zhang, Y. Zhong and D. Xing, *ACS Appl. Mater. Interfaces*, 2023, **40**, 46738–46746.
- 29 Y. Lai, J. Wang, N. Yue, Q. Zhang, J. Wu, W. Qi and R. Su, *Biomater. Sci.*, 2023, **11**, 2292–2316.
- 30 F. Qiao, J. Wang, S. Ai and L. Li, *Sens. Actuators, B*, 2015, **216**, 418–427.
- 31 Y. Huang, C. Liu, F. Pu, Z. Liu, J. Ren and X. Qu, *Chem. Commun.*, 2017, **53**, 3082–3085.
- 32 S. L. Ruizhen Tian, H. Ma, W. Ye, Y. Li, S. Wang, Z. Zhang, F. B. Mingsong Zang, J. Hou, J. Xu, Q. Luo, H. Sun, J. Liu and Y. Yang, *Adv. Funct. Mater.*, 2022, **32**, 2204025.
- 33 T. Thomas, R. J. Mascarenhas, P. Martis, Z. Mekhalif and B. E. K. Swamy, *Mater. Sci. Eng., C*, 2013, **33**, 3294–3302.
- 34 W. Yuan, G. Jiang, J. Che, X. Qi, R. Xu, M. W. Chang, Y. Chen, S. Y. Lim, J. Dai and M. B. Chan-Park, *J. Phys. Chem. C*, 2008, **112**, 18754–18759.
- 35 H. Z. Zardini, A. Amiri, M. Shanbedi, M. Maghrebi and M. Baniadam, *Colloids Surf., B*, 2012, **92**, 196–202.
- 36 M. Kumar, B. E. Kumara Swamy, S. Reddy, W. Zhao, S. Chetana and V. Gowrav Kumar, *J. Electroanal. Chem.*, 2019, **835**, 96–105.
- 37 S. A. Kumar, S. F. Wang, Y. T. Chang, H. C. Lu and C. T. Yeh, *Colloids Surf., B*, 2011, **82**, 526–531.
- 38 N. Murugan, T. H. V. Kumar, N. R. Devi and A. K. Sundramoorthy, *New J. Chem.*, 2019, **43**, 15105–15114.
- 39 Y. Wang, W. Li, H. Li, M. Ye, X. Zhang, C. Gong, H. Zhang, G. Wang, Y. Zhang and C. Yu, *Chem. Eng. J.*, 2021, **414**, 128925.
- 40 S. Mallakpour, A. Abdolmaleki and S. Borandeh, *Prog. Org. Coat.*, 2014, **77**, 1966–1971.
- 41 F. Avilés, J. V. Cauich-Rodríguez, L. Moo-Tah, A. May-Pat and R. Vargas-Coronado, *Carbon*, 2009, **47**, 2970–2975.
- 42 L. Y. Jun, N. M. Mubarak, L. S. Yon, C. H. Bing, M. Khalid and E. C. Abdullah, *J. Environ. Chem. Eng.*, 2018, **6**, 5889–5896.
- 43 Z. Zhao, Z. Yang, Y. Hu, J. Li and X. Fan, *Appl. Surf. Sci.*, 2013, **276**, 476–481.
- 44 D. Cheng, L. Yang, R. Hu, J. Liu, R. Che, J. Cui, Y. Wu, W. Chen, J. Huang, M. Zhu and Y. J. Zhao, *ACS Appl. Mater. Interfaces*, 2019, **11**, 36685–36696.
- 45 S. Xiao, Z. Li, J. Liu, Y. Song, T. Li, Y. Xiang, J. S. Chen and Q. Yan, *Small*, 2020, **16**, 1–9.
- 46 A. S. Kshirsagar, C. Hiragond, A. Dey, P. V. More and P. K. Khanna, *ACS Appl. Energy Mater.*, 2019, **2**, 2680–2691.
- 47 Z. Li, L. Yuan, Z. Yi, Y. Liu and Y. Huang, *Nano Energy*, 2014, **9**, 229–236.
- 48 J. Yuan, J. X. Mi, R. Yin, T. Yan, H. Liu, X. Chen, J. Liu, W. Si, Y. Peng, J. Chen and J. Li, *ACS Catal.*, 2022, **12**, 1024–1030.
- 49 J. Li, P. Yu, J. Xie, J. Liu, Z. Wang, C. Wu, J. Rong, H. Liu and D. Su, *ACS Catal.*, 2017, **7**, 7305–7311.
- 50 L. Ma, H. L. Zhuang, S. Wei, K. E. Hendrickson, M. S. Kim, G. Cohn, R. G. Hennig and L. A. Archer, *ACS Nano*, 2016, **10**, 1050–1059.
- 51 S. Pal, S. Bawari, T. Veetil Vineesh, N. Shyaga and T. N. Narayanan, *ACS Appl. Energy Mater.*, 2019, **2**, 3624–3632.
- 52 L. Qian, A. R. Thirupathi, J. Van Der Zalm and A. Chen, *ACS Appl. Nano Mater.*, 2021, **4**, 3696–3706.
- 53 M. Zahirul Kabir, C. Erkmén, S. Kurbanoglu, G. Aydogdu Tig and B. Uslu, *J. Electroanal. Chem.*, 2023, **944**, 117651.
- 54 N. Mavis Xhakaza, R. Chokkareddy and G. G. Redhi, *J. Mol. Liq.*, 2022, **368**, 120444.
- 55 S. N. Bhaduri, D. Ghosh, S. Chatterjee, R. Biswas, A. Bhaumik and P. Biswas, *J. Mater. Chem. B*, 2023, **11**, 8956–8965.
- 56 M. Xu, W. Wang, H. Han, Y. Wei, J. Sha and G. Liu, *Chem. Eng. J.*, 2023, **475**, 146324.

- 57 C. Liu, Y. Cai, J. Wang, X. Liu, H. Ren, L. Yan, Y. Zhang, S. Yang, J. Guo and A. Liu, *ACS Appl. Mater. Interfaces*, 2020, **12**, 42521–42530.
- 58 M. Sherazee, S. R. Ahmed, P. Das, S. Srinivasan and A. R. Rajabzadeh, *Colloids Surf., A*, 2023, **679**, 132576.
- 59 Z. Xu, P. Li, X. Liu, X. Zhu, M. Liu, Y. Zhang and S. Yao, *Electrochim. Acta*, 2022, **434**, 141273.
- 60 A. M. Mahmoud, M. H. Mahnashi and M. M. El-Wekil, *Anal. Chim. Acta*, 2023, **1272**, 341498.
- 61 A. M. Mahmoud, B. A. Alyami, M. H. Mahnashi, F. M. Alshareef, Y. S. AlQahtani and M. M. El-Wekil, *Microchem. J.*, 2023, **187**, 108419.
- 62 W. Song, B. Zhao, C. Wang, Y. Ozaki and X. Lu, *J. Mater. Chem. B*, 2019, **7**, 850–875.
- 63 X. Zhou, L. Kong, J. Hao, J. Feng, S. Sun, C. Zhou, Y. Liu, Z. Yan, X. Zhu and L. Hu, *J. Mater. Chem. C*, 2023, **11**, 13047–13055.
- 64 M. Sun, K. Pu, X. Hao, T. Liu, Z. Lu, G. Su, C. Wu, Y. Wang, S. Cai, X. Zhao and H. Rao, *J. Mater. Chem. C*, 2023, **12**, 221–231.
- 65 A. R. Hormozi Jangi, M. R. Hormozi Jangi and S. R. Hormozi Jangi, *Chin. J. Chem. Eng.*, 2020, **28**, 1492–1503.
- 66 N. Lu, Y. Liu, X. Yan, Z. Xu, Y. Xing, Y. Song, P. Zhao, M. Liu, Y. Gu, Z. Zhang and S. Zhai, *ACS Appl. Nano Mater.*, 2022, **8**, 11361–11370.